COMMUN. MATH. SCI.
Vol. 17, No. 8, pp. 2309–2324

BUBBLE ASSEMBLIES IN TERNARY SYSTEMS WITH LONG RANGE INTERACTION*

CHONG WANG†, XIAOFENG REN‡, AND YANXIANG ZHAO§

Abstract. A nonlocal diffuse interface model, based on the Nakazawa-Ohta density functional theory for triblock copolymers, is used to study bubble assemblies in ternary systems. The model has three parameters weighing three types of long-range interaction and two parameters that fix the total area of each constituent. As the parameters vary, a large number of morphological phases appear as stable stationary states. One open question related to the polarity direction of double bubble assemblies is answered numerically. Moreover, it is shown that the average size of bubbles in a single bubble assembly depends on the sum of the minority constituent areas and the long-range interaction coefficients. One further identifies the ranges for area fractions and the long-range interaction coefficients for double bubble assemblies.

Keywords. Diffuse interface model; Nakazawa-Ohta density functional; Triblock copolymers; Morphological phases; Long-range interaction.

AMS subject classifications. 82D60; 92C15; 74N20; 35R35; 70E55.

1. Introduction

Block copolymers have generated much interest in materials science in recent years due to their remarkable ability for self-assembly into nanoscale ordered structures [1–3]. This ability can be exploited to create materials with desired mechanical, optical, electrical, and magnetic properties [1–3]. There have been many experimental and theoretical studies focusing on this subject [4–13]. Self-consistent field theory derived from a microscopic description of interacting polymer chains is one successful theoretical approach for the study of block copolymers [5–11]. However, this method is computationally demanding because of the heavy calculation of path integrals for the chain conformation [14,15]. There is a need for efficient methods to model the self-assembly for block copolymers at the mesoscale level. The density functional theory (DFT) [16,17] is a very promising approach to modeling such phenomena and it is customarily referred to as cell dynamics simulation [12,13].

In this paper, we consider the Ohta-Nakazawa model introduced in [17], which describes the ternary system such as ABC-type triblock copolymers by a free energy functional written as follows:

$$E(\phi_1,\phi_2)=\int_D\left[\frac{\epsilon}{2}\left(|\nabla\phi_1|^2+|\nabla\phi_2|^2+\nabla\phi_1\cdot\nabla\phi_2\right)+\frac{1}{2\epsilon}W_T(\phi_1,\phi_2)\right]dx$$
$$+\sum_{i,j=1}^{2}\frac{\gamma_{ij}}{2}\int_D\left[(-\triangle)^{-\frac{1}{2}}\left(f(\phi_i)-\omega_i\right)\times(-\triangle)^{-\frac{1}{2}}\left(f(\phi_j)-\omega_j\right)\right]dx. \tag{1.1}$$

where $0<\epsilon\ll 1$ is an interface parameter, indicating that the system is in the strong segregation regime [13]. $D\subset\mathbb{R}^n$, $n=2,3$ is a spatial domain, and $\phi_i=\phi_i(x)$ $(i=1,2)$ are

*Received: September 16, 2018; Accepted (in revised form): September 3, 2019. Communicated by Qiang Du.

†Department of Mathematics and Statistics, McMaster University, Hamilton, Ontario, L8S 4K1, Canada (wangc196@mcmaster.ca).

‡Department of Mathematics, The George Washington University, Washington D.C., 20052, USA (ren@gwu.edu).

§Corresponding author. Department of Mathematics, The George Washington University, Washington D.C., 20052, USA (yxzhao@gwu.edu).

phase field labeling functions which represent the density of A and B species, respectively. The concentration of C species can be implicitly represented by $1-\phi_1(x)-\phi_2(x)$ since the system is assumed to be incompressible [16]. $W_T(\phi_1,\phi_2)$ is of the form of

$$W_T(\phi_1,\phi_2) := W(\phi_1)+W(\phi_2)+W(1-\phi_1-\phi_2),$$

where $W(s)=18(s^2-s)^2$. Note that $W_T(\phi_1,\phi_2)$ is a triple-well potential having three minima at $(1,0,0)$, $(0,1,0)$ and $(0,0,1)$, which correspond to the phase separation between the A,B,C species. The first integral in (1.1) describes the short-range interaction which accounts for the interfacial free energy of the system and favors large domains with minimum surface area.

The second integral term in (1.1) indicates the long-range interaction between the chain molecules with γ_{ij} being the strength of such interactions. The long-range interaction coefficients γ_{ij} form a symmetric two by two matrix $\gamma=[\gamma_{ij}]$. For triblock copolymers, the matrix γ is positive definite [18]; for homopolymer/diblock copolymer blends γ has one positive eigenvalue and one zero eigenvalue [19]. In our work, we study the effect of γ in a wide range, including positive definite and non-positive definite cases. The new introduced term

$$f(\phi_i)=3\phi_i^2-2\phi_i^3, \quad i=1,2 \tag{1.2}$$

is adapted to mimic $\phi_i, i=1,2$ as the indicator for the A and B species, respectively. $\omega_i\in(0,1), i=1,2$ are the relative volumes of the A and B species, respectively, which indicate that the Ohta-Nakazawa model is usually associated with volume constraints:

$$\int_D f(\phi_i)dx=\omega_i|D|, \quad i=1,2. \tag{1.3}$$

The negative square root of $-\Delta$ is defined in Section 3 in details.

The importance of the new introduced term $f(\phi_i)$ is due to two reasons. Firstly, heuristically, with such a function, we have not only $f(0)=0, f(1)=1$ which resembles the behavior of ϕ_i, but also that

$$f'(0)=0, \quad f'(1)=0. \tag{1.4}$$

These will lead to a more localized 'boundary force' near the A-C, B-C and A-B interfaces. On the other hand, if taking $f(s)=s$, then $f'(s)=1$ will induce a local surface tension force against a global long-range repulsive force. To balance such two forces, the ϕ_i has to sacrifice by losing the desired tanh profile (a hyperbolic tangent shape which monotonically changes its value from 0 to 1) and results in either unphysical negative values in the proximity of the interface (see [20]) or values not equal to 0 or 1 away from the interface [21]. Secondly, since the new $f(\phi_i)$ results in a much better tanh profile, consequently the new model will describe the interfacial structures more accurately and lead to a better estimate of the free energy.

Now we consider the dynamic problem of the L^2 gradient flow

$$\begin{aligned}\frac{\partial\phi_i}{\partial t}=-\frac{\delta E}{\delta\phi_i}=&\ \epsilon\triangle\phi_i+\frac{\epsilon}{2}\triangle\phi_j-\frac{1}{2\epsilon}\frac{\partial W_T}{\partial\phi_i}\\ &-\gamma_{ii}(-\triangle)^{-1}(f(\phi_i)-\omega_i)f'(\phi_i)-\gamma_{ij}(-\triangle)^{-1}(f(\phi_j)-\omega_j)f'(\phi_i)-\lambda_i(t)f'(\phi_i)\end{aligned} \tag{1.5}$$

in which $i,j=1,2$ and $j\neq i$. Here $\lambda_i(t)$ is some appropriate time-dependent Lagrange multiplier associated with the volume constraints (1.3). The L^2 gradient flow dynamics

will lead us to a variety of equilibrium configurations. On the other hand, to see how the volume constraints (1.3) play a role in the energy minimization, we can alternatively incorporate the penalty term in (1.1) and change it into an unconstrained one:

$$\begin{aligned} E_{\text{penalty}}(\phi_1,\phi_2) = &\int_D \left[\frac{\epsilon}{2}\left(|\nabla\phi_1|^2+|\nabla\phi_2|^2+\nabla\phi_1\cdot\nabla\phi_2\right)+\frac{1}{2\epsilon}W_T(\phi_1,\phi_2)\right]dx \\ &+\sum_{i,j=1}^{2}\frac{\gamma_{ij}}{2}\int_D\left[(-\triangle)^{-\frac{1}{2}}(f(\phi_i)-\omega_i)\times(-\triangle)^{-\frac{1}{2}}(f(\phi_j)-\omega_j)\right]dx \\ &+\sum_{i=1}^{2}\frac{M_i}{2}\left(\int_D f(\phi_i)dx-\omega_i|D|\right)^2, \end{aligned} \tag{1.6}$$

and consider the corresponding penalized L^2 gradient flow dynamics:

$$\begin{aligned} \frac{\partial\phi_i}{\partial t} = -\frac{\delta E_{\text{penalty}}}{\delta\phi_i} = &\epsilon\triangle\phi_i+\frac{\epsilon}{2}\triangle\phi_j-\frac{1}{2\epsilon}\frac{\partial W_T}{\partial\phi_i} \\ &-\gamma_{ii}(-\triangle)^{-1}(f(\phi_i)-\omega_i)f'(\phi_i)-\gamma_{ij}(-\triangle)^{-1}(f(\phi_j)-\omega_j)f'(\phi_i) \\ &-M_i\left(\int_D f(\phi_i)dx-\omega_i|D|\right)f'(\phi_i). \end{aligned} \tag{1.7}$$

When $M_i\to\infty$, $M_i\left(\int_D f(\phi_i)dx-\omega_i|D|\right)$ approaches the Lagrange multiplier $\lambda_i(t)$ which makes the penalized L^2 gradient flow dynamics (1.7) consistent with the dynamics (1.5) [22]. Throughout this paper, we will focus on the penalized L^2 gradient flow (1.7) to study the configurations of minimizers of (1.6).

As $\epsilon\to 0$, the free energy (1.1) Γ-converges to the strong segregation limit (sharp interface limit) [23–28]

$$\mathcal{J}(\Omega_1,\Omega_2)=\frac{1}{2}\sum_{i=1}^{3}\mathcal{P}_D(\Omega_i)+\sum_{i,j=1}^{2}\frac{\gamma_{ij}}{2}\int_D\left[(-\Delta)^{-1/2}(\chi_{\Omega_i}-\omega_i)\times(-\Delta)^{-1/2}(\chi_{\Omega_j}-\omega_j)\right]dx, \tag{1.8}$$

where $\Omega_i\subset D$ denotes the region covered by the i-th constituent and the measure of Ω_i is fixed at

$$|\Omega_i|=\omega_i|D|. \tag{1.9}$$

$\mathcal{P}_D(\Omega_i)$ denotes the perimeter of Ω_i in D which is defined as the total variation of the function χ_{Ω_i} (see (2.1) for the definition) and χ_{Ω_i} is the characteristic function of Ω_i, that is, $\chi_{\Omega_i}(x)=1$ if $x\in\Omega_i$ and 0 if $x\in D\setminus\Omega_i$.

We address small volume-fraction asymptotic analysis ($\omega_i\ll 1$) of the sharp interface model. We then design and implement stable and accurate numerical methods for solving the penalized L^2 gradient flow Equation (1.7). Our methods couple a linear operator-splitting technique and spectral discretization which leads to a stabilized numerical scheme for (1.7). We apply our model and numerical methods to the triblock copolymer systems with $\omega_i\ll 1$, from which we find patterns such as hexagonal double bubble assemblies, square single bubble assemblies and double bubble and single bubble coexisting states. We perform quantitative studies on these numerical results and verify them theoretically through the sharp interface approach.

The rest of the paper is organized as follows. In Section 2, we perform asymptotic analysis for the sharp interface model. In Section 3, we describe our numerical methods

for solving the gradient flow dynamic equations of the penalized phase field free energy functional. In Section 4 we present numerous equilibrium configurations as parameters vary. Moreover, we provide quantitative studies and verify them theoretically. Section 5 gives the conclusion and future directions.

2. Sharp interface model: asymptotic analysis

A function $f \in L^1(D)$ is said to have bounded variation in D if $\int_D |\nabla f| < \infty$, where

$$\int_D |\nabla f| := \sup\left\{ \int_D f \operatorname{div} \mathbf{g}\, dx : \mathbf{g} = (g_1, \cdots, g_n) \in C_c^1(D, \mathbb{R}^n), \text{ and } |\mathbf{g}(x)| \le 1 \text{ for } x \in D \right\},$$

is the total variation of f and $C_c^1(D,\mathbb{R}^n)$ denotes the space of all C^1-mappings from D to $\mathbb{R}^n$ that are compactly supported inside D; cf. [29–31]. If $f \in W^{1,1}(\Omega)$, then

$$\int_D |\nabla f| = \int_D |\operatorname{grad} f| dx,$$

where $\operatorname{grad} f = (f_1, \cdots, f_n)$ and $f_1, \cdots, f_n$ are the generalized derivatives of f. Then the space $BV(D)$ is defined as the space of all functions in $L^1(D)$ with bounded variation. It is a Banach space with the norm

$$||f||_{BV(D)} := ||f||_{L^1} + \int_D |\nabla f|.$$

If Ω is Lebesgue measurable, then the perimeter of Ω in D is defined by the total variation of the function χ_Ω [29–31], that is,

$$\mathcal{P}_D(\Omega) := \int_D |\nabla \chi_\Omega| = \sup\left\{ \int_\Omega \operatorname{div} \mathbf{g}\, dx : \mathbf{g} \in C_c^1(D, \mathbb{R}^n), |\mathbf{g}(x)| \le 1 \right\}. \tag{2.1}$$

A stationary point (Ω_1, Ω_2) of $\mathcal{J}$ (1.8) consists of two disjoint subsets Ω_1 and Ω_2 of D, each bounded by piecewise smooth curves. It satisfies the following equations:

$$\kappa_1 + \gamma_{11} I_{\Omega_1} + \gamma_{12} I_{\Omega_2} = \lambda_1 \quad \text{on } \partial\Omega_1 \cap \partial\Omega_3 \tag{2.2}$$

$$\kappa_2 + \gamma_{12} I_{\Omega_1} + \gamma_{22} I_{\Omega_2} = \lambda_2 \quad \text{on } \partial\Omega_2 \cap \partial\Omega_3 \tag{2.3}$$

$$\kappa_0 + (\gamma_{11} - \gamma_{12}) I_{\Omega_1} + (\gamma_{12} - \gamma_{22}) I_{\Omega_2} = \lambda_1 - \lambda_2 \quad \text{on } \partial\Omega_1 \cap \partial\Omega_2 \tag{2.4}$$

$$T_1 + T_2 + T_0 = \vec{0} \quad \text{at } \partial\Omega_1 \cap \partial\Omega_2 \cap \partial\Omega_3 \tag{2.5}$$

$$T_i \perp \partial D \text{ at } \overline{\partial\Omega_i \cap \partial\Omega_3} \cap \partial D,\ i = 1,2 \tag{2.6}$$

$$T_0 \perp \partial D \text{ at } \overline{\partial\Omega_1 \cap \partial\Omega_2} \cap \partial D. \tag{2.7}$$

The Equation (2.2) holds on $\partial\Omega_1 \cap \partial\Omega_3$ which is the interface between Ω_1 and Ω_3. On the left side of (2.2) κ_1 is the curvature of this interface with respect to the normal vector that points inward into Ω_1. The I_{Ω_i}'s are shorthand notations:

$$I_{\Omega_i} = (-\Delta)^{-1}(\chi_{\Omega_i} - \omega_i),\ i = 1,2, \tag{2.8}$$

which we call inhibitors. The Equations (2.3) holds on the interface between Ω_2 and Ω_3 and the curvature κ_2 is measured with respect to the normal vector pointing into Ω_2; the Equation (2.4) holds on the interface between Ω_1 and Ω_2 and the curvature κ_0 is measured with respect to the normal vector pointing into Ω_1. On the right sides of these equations there are unknown constants λ_1 and λ_2. These are Lagrange multipliers associated with the constraints $|\Omega_i| = \omega_i |D|$, $i = 1,2$.

The three interfaces, $\partial\Omega_1\cap\partial\Omega_3$, $\partial\Omega_2\cap\partial\Omega_3$ and $\partial\Omega_1\cap\partial\Omega_2$, may meet at a common point in D, which is termed a triple junction point. In (2.5), T_1, T_2 and T_0 are unit tangent vectors of the curves $\partial\Omega_1\cap\partial\Omega_3$, $\partial\Omega_2\cap\partial\Omega_3$, and $\partial\Omega_1\cap\partial\Omega_2$ at triple junction points: T_1 is inward pointing (pointing towards the interior of the curve) and tangent to $\partial\Omega_1\cap\partial\Omega_3$, T_2 is inward pointing and tangent to $\partial\Omega_2\cap\partial\Omega_3$, and T_0 is inward pointing and tangent to $\partial\Omega_1\cap\partial\Omega_2$; see Figure 2.1. The Equation (2.5) is equivalent to the condition that at any triple junction point the three interfaces meet at 120 degrees.

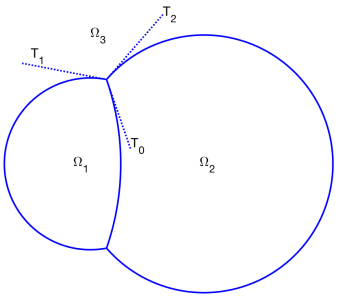

FIG. 2.1. *Unit tangent vectors T_1, T_2 and T_0.*

In the case that an interface meets the domain boundary ∂D, the Equations (2.6) and (2.7) assert that it does so perpendicularly. Here T_1, T_2 and T_0 are again unit tangent vectors of $\partial\Omega_1\cap\partial\Omega_3$, $\partial\Omega_2\cap\partial\Omega_3$ and $\partial\Omega_1\cap\partial\Omega_2$ respectively.

It is convenient to introduce a fixed $m\in(0,1)$ and a small η so that

$$\omega_1|D|=\eta^2 m \text{ and } \omega_2|D|=\eta^2(1-m). \tag{2.9}$$

The area constraints (1.9) now take the form

$$|\Omega_1|=\eta^2 m \text{ and } |\Omega_2|=\eta^2(1-m). \tag{2.10}$$

Instead of ω_1 and ω_2, η becomes one parameter. The fixed number m measures the relative size of $|\Omega_1|$ vs $|\Omega_2|$ since $\frac{|\Omega_1|}{|\Omega_2|}=\frac{m}{1-m}$.

In two dimensions, currently only three types of stationary assembly were known for ternary systems: the double bubble assembly [32], the core-shell assembly [33] and the single bubble assembly [34]. In a double bubble assembly each component is a perturbed double bubble where one of the bubbles is made of type-A constituent and the other of type-B constituent and in a single bubble assembly each component is a perturbed single bubble made of either type-A or type-B constituent; see Figure 2.2. In our earlier work, we have shown the existence of a double bubble assembly and the existence of a single bubble assembly. Here we list the results as follows. One can refer to [32,34] for detailed proofs.

THEOREM 2.1 ([34]). *Let D be a bounded and sufficiently smooth domain in $\mathbb{R}^2$. For $m\in(0,1)$, $K_1,K_2\in\mathbb{N}$, $\delta>0$, and $B>0$, there exists $\eta_0=\eta_0(D,m,K_1,K_2,\delta,B)>0$ so that if*

(1) $0<\eta<\eta_0$,

(2) each entry $\gamma_{ij}>0$ and each diagonal entry $\gamma_{ii}\in\left(\frac{1+\delta}{\rho_i^3\log\frac{1}{\rho_i}},\frac{12-\delta}{\rho_i^3}\right)$, where $\rho_1=\eta(\frac{m}{K_1\pi})^{1/2}$ and $\rho_2=\eta(\frac{1-m}{K_2\pi})^{1/2}$,

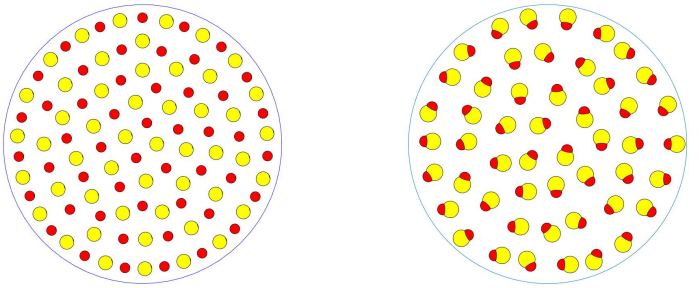

FIG. 2.2. *Left: schematic for a single bubble assembly of type-A (red) constituent and type-B (yellow) constituent. Right: schematic for a double bubble assembly.*

(3) $\frac{\max\{\gamma_{ij}\}}{\min\{\gamma_{ij}\}} < B$,

then $\mathcal{J}$ *admits a stable stationary assembly of* K_1 *perturbed single bubbles of type-A and* K_2 *perturbed single bubbles of type-B, satisfying (2.2), (2.3), and (2.10).*

Moreover, the radii of the type-A single bubbles in the assembly are close to ρ_1 *and the radii of the type-B single bubbles are close to* ρ_2*. If*

$$\frac{\gamma_{ij}}{|\gamma|} \to \Gamma_{ij} \text{ as } \eta \to 0,$$

the centers of the type-A single bubbles are $\xi_1^{*,1},\dots,\xi_1^{*,K_1}$*, and the centers of the type-B single bubbles are* $\xi_2^{*,1},\dots,\xi_2^{*,K_2}$*, then* $(\xi_1^{*,1},\dots,\xi_1^{*,K_1},\xi_2^{*,1},\dots,\xi_2^{*,K_2})$ *is close to a minimum of the function*

$$\begin{aligned} F_s(\xi_1^1,\dots,\xi_1^{K_1},\xi_2^1,\dots,\xi_2^{K_2}) = {} & \frac{\Gamma_{11}m^2}{K_1^2}\Big(\sum_{k=1}^{K_1} R(\xi_1^k,\xi_1^k) + \sum_{k=1}^{K_1}\sum_{l=1,l\neq k}^{K_1} G(\xi_1^k,\xi_1^l)\Big) \\ & + \frac{2\Gamma_{12}m(1-m)}{K_1K_2}\sum_{k=1}^{K_1}\sum_{l=1}^{K_2} G(\xi_1^k,\xi_2^l) \\ & + \frac{\Gamma_{22}(1-m)^2}{K_2^2}\Big(\sum_{k=1}^{K_2} R(\xi_2^k,\xi_2^k) + \sum_{k=1}^{K_2}\sum_{l=1,l\neq k}^{K_2} G(\xi_2^k,\xi_2^l)\Big). \end{aligned}$$

THEOREM 2.2 ([32]). *Let* D *be a bounded and sufficiently smooth domain in* $\mathbb{R}^2$*. For* $m\in(0,1)$*,* $K\in\mathbb{N}$*,* $\iota\in(0,1]$*, there exists* $\eta_0=\eta_0(D,m,K,\iota)>0$*,* $\tilde{\sigma}=\tilde{\sigma}(D,m,K,\iota)>0$*, and* $\sigma=\sigma(D,m,K,\iota)>0$*, so that if*

(1) $0<\eta<\eta_0$,

(2) $\frac{\tilde{\sigma}}{\eta^3\log\frac{1}{\eta}} \le \bar{\lambda}(\gamma) \le \bar{\bar{\lambda}}(\gamma) < \frac{\sigma}{\eta^3}$,

(3) $\iota\bar{\bar{\lambda}}(\gamma) \le \bar{\lambda}(\gamma)$,

then $\mathcal{J}$ *admits a stable stationary assembly of* K *perturbed double bubbles satisfying (2.2)-(2.5) and (2.10). Each perturbed double bubble is bounded by three smooth curves that meet at two triple junction points.*

Moreover, all the perturbed double bubbles in the solution have almost the same size and shape. If the perturbed double bubbles in the solution are located at points

$\xi^{*,1},\xi^{*,2},...,\xi^{*,K}$, then $\xi^{*,1},\xi^{*,2},...,\xi^{*,K}$ is close to a minimum of the function

$$F_d(\xi^1,\xi^2,...,\xi^K)=\sum_{k=1}^{K}R(\xi^k,\xi^k)+\sum_{k=1}^{K}\sum_{l=1,l\neq k}^{K}G(\xi^k,\xi^l).$$

The smoothness condition on D in Theorem 2.1 and Theorem 2.2 is to ensure that $(-\Delta)^{-1}$ is well defined; any $C^{2,\alpha}$ domain meets the requirement [35, Section 6.7]. Note that in Theorem 2.1, ρ_1 and ρ_2 are the average radii of the type-A and type-B discs respectively; in Theorem 2.2, $\bar{\lambda}(\gamma)$ and $\bar{\bar{\lambda}}(\gamma)$ are two eigenvalues of γ. $|\gamma|$ is the operator norm of γ. The definition of functions F_s and F_d involve G and R. Here G is the Green's function of $-\triangle$ operator on D with either periodic or homogeneous Neumann boundary condition. The function $G(x,y)$ as a function of x for each $y\in D$ solves

$$-\triangle G(\cdot,y)=\delta(\cdot-y)-\frac{1}{|D|},\ \int_D G(x,y)dx=0. \tag{2.11}$$

One can write G as a sum of two terms:

$$G(x,y)=\frac{1}{2\pi}\log\frac{1}{|x-y|}+R(x,y). \tag{2.12}$$

The first term $\frac{1}{2\pi}\log\frac{1}{|x-y|}$ is the fundamental solution of the Laplace operator; the second term R is the regular part of the Green's function, a smooth function of $(x,y)\in D\times D$. In the case that D is the unit disc,

$$G(x,y)=\frac{1}{2\pi}\log\frac{1}{|x-y|}+\frac{1}{2\pi}\left[\frac{|x|^2}{2}+\frac{|y|^2}{2}+\log\frac{1}{|x\overline{y}-1|}\right]-\frac{3}{8\pi}, \tag{2.13}$$

where $\overline{y}$ is the complex conjugate of y and D is viewed as a subset of $\mathbb{C}$, so we have a closed formula for both F_s and F_d.

The primary difference of Theorem 2.1 and Theorem 2.2 lies on the matrix γ. In Theorem 2.1, all the entries of γ should be positive and comparable. The matrix γ can be positive definite or not. In Theorem 2.2, the matrix γ should be positive definite and the two eigenvalues of γ need to be comparable.

When (Ω_1,Ω_2) is a stationary single bubble assembly found in Theorem 2.1, the free energy in the strong segregation limit $\mathcal{J}(\Omega_1,\Omega_2)$ in (1.8) becomes:

$$\begin{aligned}\mathcal{J}(S_1,S_2)=&\sum_{i=1}^{2}\sum_{k=1}^{K_i}\left(2\pi(r_i^k)+\frac{\gamma_{ii}\pi}{4}(r_i^k)^4\log\frac{1}{r_i^k}\right)+\sum_{i=1}^{2}\sum_{k=1}^{K_i}\frac{\gamma_{ii}\pi^2}{2}(r_i^k)^4\left(\frac{1}{8\pi}+R(\xi_i^k,\xi_i^k)\right)\\&+\sum_{i=1}^{2}\sum_{\substack{k,l=1\\k\neq l}}^{K_i}\frac{\gamma_{ii}\pi^2}{2}\left(r_i^k\right)^2\left(r_i^l\right)^2G(\xi_i^k,\xi_i^l)+\gamma_{12}\pi^2\sum_{k=1}^{K_1}\sum_{l=1}^{K_2}(r_1^k)^2(r_2^l)^2G(\xi_1^k,\xi_2^l)+O(|\gamma|\eta^6).\end{aligned} \tag{2.14}$$

Here (S_1,S_2) is an assembly of perturbed single bubbles at equilibrium.

An assembly of perfect single bubbles is used as an approximate solution, and then one proves that small and suitable perturbations of the single bubbles will turn the assembly to an equilibrium of the nonlocal system. Thus the existence of single bubble assemblies is theoretically established [34]. The free energy (2.14) gives rise to (4.2) up to the leading order which is used to verify the relationship (4.1) in Section 4.2.

When (Ω_1,Ω_2) is a stationary double bubble assembly found in Theorem 2.2, the free energy in the strong segregation limit $\mathcal{J}(\Omega_1,\Omega_2)$ in (1.8) reads:

$$\begin{aligned}\mathcal{J}(D_1,D_2)=&\eta\sum_{k=1}^{K_b}\sum_{i=0}^{2}a_i^k l_i^k+\eta^4\log\frac{1}{\eta}\sum_{k=1}^{K_b}\sum_{i,j=1}^{2}\frac{\gamma_{ij}w_i^k w_j^k}{4\pi}\\&+\eta^4\sum_{k=1}^{K_b}\sum_{i,j=1}^{2}\frac{\gamma_{ij}}{2}\int_{B_i^k}\int_{B_j^k}\frac{1}{2\pi}\log\frac{1}{|\hat{x}-\hat{y}|}d\hat{x}d\hat{y}+\eta^4\sum_{k=1}^{K_b}\sum_{i,j=1}^{2}\frac{\gamma_{ij}}{2}w_i^k w_j^k R(\xi_k,\xi_k)\\&+\eta^4\sum_{\substack{k,l=1\\k\neq l}}^{K_b}\sum_{i,j=1}^{2}\frac{\gamma_{ij}}{2}w_i^k w_j^l G(\xi_k,\xi_l)+o(|\gamma|\eta^4).\end{aligned}\tag{2.15}$$

Here the equilibrium (D_1,D_2) is an assembly of perturbed double bubbles. Each double bubble is built from an exact double bubble (B_1^k,B_2^k) whose three radii are $l_i^k, i=0,1,2$ and two areas are w_1^k and w_2^k. There is a transformation

$$T_k:\hat{x}\to\eta e^{\mathrm{i}\theta_k}\hat{x}+\xi_k$$

that maps (B_1^k,B_2^k) to $(T(B_1^k),T(B_2^k)$ in the domain and (D_1,D_2) is a perturbation of $\cup_{k=1}^{K_b}(T(B_1^k),T(B_2^k))$. Here $\hat{x}\in\mathbb{R}^2$ and we identify $\mathbb{R}^2$ with $\mathbb{C}$ to perform the complex multiplication. In T_k, ξ_k and θ_k are the center and the direction of the double bubble respectively. The free energy (2.15) results in (4.4) up to the leading order which is used to verify the two-thirds law (4.5) in Section 4.2.

3. Numerical methods

In this section we describe our numerical methods for solving the Equation (1.7) in two dimensions (2D). Our computational domain is taken as $D=[-L_x,L_x]\times[-L_y,L_y]$ in $\mathbb{R}^2$.

3.1. Notations. Let $D=\prod_{i=1}^{d}[-X_i,X_i)\subset\mathbb{R}^d, d=2,3$ be a periodic domain. Denote the space consisting of periodic functions in $H^s(D), s\geq 0$ as $H^s_{\mathrm{per}}(D)$. We define the subspaces

$$\mathring{H}^s_{\mathrm{per}}(D):=\left\{u\in H^s_{\mathrm{per}}(D):\int_D u(x)dx=0\right\}\tag{3.1}$$

consisting of all functions of $u\in H^s_{\mathrm{per}}(D)$ with zero mean. We use $\|\cdot\|_{H^s}$ to represent the standard Sobolev norm. When $s=0$, $H^s(D)=L^2(D)$ and we take $\langle\cdot,\cdot\rangle$ as the L^2 inner product and $\|\cdot\|_{H^s}=\|\cdot\|_{L^2}$.

We define the inverse Laplacian $(-\Delta)^{-1}$: $\mathring{L}^2_{\mathrm{per}}(D)\to\mathring{H}^1_{\mathrm{per}}(D)$ as

$$(-\Delta)^{-1}g=u\Longleftrightarrow-\Delta u=g.$$

or in terms of Fourier series:

$$(-\Delta)^{-1}g=\sum_{k\in\mathbb{Z}^3\setminus\{0\}}|k|^{-2}\hat{g}(k)e^{\mathrm{i}k\cdot\tilde{x}},\tag{3.2}$$

where

$$\hat{g}(k)=\int_D f(x)e^{-\mathrm{i}k\cdot\tilde{x}}dx,\quad\text{with}\quad\tilde{x}=(\pi x_1/X_1,\cdots,\pi x_d/X_d).$$

Note that the definition (3.2) can be extended to any function $g\in L^2_{\mathrm{per}}(D)$ because of the removal of the zeroth mode.

3.2. Linear splitting and semi-discrete scheme. We adopt an analogous linear splitting scheme which has been used in designing stabilized numerical methods for the classic Allen-Cahn equation [20, 22, 36–38]. We rewrite $\frac{\partial W_T}{\partial \phi_i}$ as

$$\frac{\partial W_T}{\partial \phi_i} = \kappa\phi_i + \left[\frac{\partial W_T}{\partial \phi_i} - \kappa\phi_i\right]. \tag{3.3}$$

Plug (3.3) into (1.7), we get an equivalent formulation

$$\frac{\partial \phi_i}{\partial t} = \epsilon\triangle\phi_i - \frac{\kappa}{2\epsilon}\phi_i + B_i(\phi_1,\phi_2), \quad i=1,2, \tag{3.4}$$

where

$$\begin{aligned} B_i(\phi_1,\phi_2) = {} & \frac{\epsilon}{2}\triangle\phi_j - \frac{1}{2\epsilon}\left(\frac{\partial W_T}{\partial \phi_i} - \kappa\phi_i\right) \\ & - \gamma_{ii}(-\triangle)^{-1}(f(\phi_i)-\omega_i)f'(\phi_i) - \gamma_{ij}(-\triangle)^{-1}(f(\phi_j)-\omega_j)f'(\phi_i) \\ & - M_i\left(\int_D f(\phi_i)dx - \omega_i|D|\right)f'(\phi_i), \end{aligned} \tag{3.5}$$

in which $i,j=1,2$ and $j\neq i$.

We choose a time step $\Delta t>0$ and set $t_n = n\Delta t$, $(n=0,1,\cdots)$. For a given function $\phi_i(x)$, we denote by ϕ_i^n an approximation of $\phi_i(x)$ at time t_n. We use the semi-implicit splitting scheme to discretize the time variable for Equations (3.4):

$$\frac{\phi_i^{n+1}-\phi_i^n}{\Delta t} = \epsilon\triangle\phi_i^{n+1} - \frac{\kappa}{2\epsilon}\phi_i^{n+1} + B_i(\phi_1^n,\phi_2^n), \tag{3.6}$$

for $i=1,2$. In our numerical simulation, we take $\kappa=72$.

3.3. Spectral spatial discretization with periodic boundary condition. Consider our rectangular domain $D\subset\mathbb{R}^2$

$$D=\{-L_x<x<L_x,-L_y<y<L_y\}$$

with periodic boundary condition for some positive numbers L_x and L_y. Let N_x,N_y be even integers. We discretize D by a rectangular mesh which is uniform in each direction as follows:

$$\mathbf{x}_{jk} = (x_j,y_k) = (-L_x+jh_x,-L_y+kh_y)$$

for $0\le j\le N_x$, $0\le k\le N_y$, $h_x=2L_x/N_x$, $h_y=2L_y/N_y$. Let $\phi_{i,jk}^n\approx\phi_i(x_j,y_k,t_n)=\phi_i(\mathbf{x}_{jk},t_n)$ denote the approximate solution at grid $\mathbf{x}_{jk}$ and time t_n. Denote the approximate solution in array form as $\Phi_i=(\phi_{jk})_{0:N_x-1,0:N_y-1}$, and denote its discrete Fourier transform (DFT) by $\hat{\Phi}_i=(\hat{\phi}_{jk})_{0:N_x-1,0:N_y-1}$. Notice that the Laplacian operator Δ in the spectral space corresponds to the spectrum

$$\lambda_{jk} = -\lambda_x^2(j) - \lambda_y^2(k),$$

where

$$\lambda_x(j) = \begin{cases} \pi j/L_x & \text{if } 0\le j\le N_x/2, \\ \pi(N_x-j)/L_x & \text{if } N_x/2\le j\le N_x-1, \end{cases}$$

$$\lambda_y(k)=\begin{cases}\pi k/L_y & \text{if } 0\le k\le N_y/2,\\ \pi(N_y-k)/L_y & \text{if } N_y/2\le k\le N_y-1,\end{cases}$$

Taking the fast Fourier transform (FFT) [39] on both sides of the Equation (3.6) yields

$$\mathbf{L}\odot\hat{\Phi}_i^{n+1}=\hat{\Phi}_i^n+\widehat{B_i(\phi_1^n,\phi_2^n)\Delta t},\quad i=1,2, \tag{3.7}$$

where $\mathbf{L}\odot\hat{\Phi}_i^{n+1}$ is given by

$$\mathbf{L}\odot\hat{\Phi}_i^{n+1}=(l_{jk}\hat{\phi}_{i,jk}^{n+1})_{0:N_x-1,0:N_y-1},\ \text{with}\ \ l_{jk}=1+\epsilon\lambda_{jk}\Delta t+\frac{\kappa}{2\epsilon}\Delta t.$$

Then $\hat{\Phi}_i^{n+1}$ can be solved from Equation (3.7) and Φ_i^{n+1} is obtained by performing inverse FFT on $\hat{\Phi}_i^{n+1}$.

4. Numerical results

The five parameters, γ_{11}, γ_{12}, γ_{22}, ω_1, and ω_2, play the key roles in pattern formation of ternary systems. In numerical simulations, the domain D is fixed as $[-1,1]^2$, the uniform mesh grid in space is fixed as 512×512, namely, $\Delta x=\Delta y=2/512$, ϵ is fixed as $5\Delta x$, $M_1=M_2=10$, $\kappa=72$, and the time step Δt is 0.001. In each image below, red, yellow and blue colors correspond to A-rich, B-rich and C-rich regions, respectively.

4.1. Sample equilibria. Two sample equilibria are presented in Figure 4.1. Figure 4.1(a) shows a double bubble assembly. All double bubbles grow into the same size and are located hexagonally. The polarity direction of each double bubble, the direction from center of mass of yellow region to that of red one, in an assembly is unknown theoretically [32]. Numerical simulations show double bubble assemblies when $|\gamma_{12}|$ is small, and the polarity directions of double bubbles in equilibrium configurations are parallel. Figure 4.1(b) shows a single bubble assembly. All yellow bubbles become equal in size, as do red bubbles. Interestingly, they form a square lattice pattern in which each single bubble is surrounded by four bubbles of the other color. In a binary system, a hexagon pattern is most stable experimentally [40] and theoretically [16, 41–44]. For a ternary system, our numerical simulations show that a square structure can be energetically more favorable than a hexagonal one, which agrees with the experimental findings [45] and theoretical studies [17,46,47]. More excitingly, a recent work in [48] has theoretically verified the square lattice pattern obtained from our numerical simulation.

4.2. Single bubble assemblies. For single bubble assemblies, the average size of red/yellow bubbles does not depend on the ratio of area fractions, namely, ω_1/ω_2. In Figure 4.2(a), for several (ω_1,ω_2) and fixed $\gamma_{ij}=20{,}000$, $1\le i,j\le2$, the ratio r_1/r_2 remains at 1/1 up to a 3% error regardless of the different values of ω_1/ω_2. Note that (ω_1,ω_2) has an impact on the number of red/yellow bubbles, as seen in the insets of Figure 4.2(a). On the other hand, the values of γ_{11} and γ_{22} affect r_1/r_2. In Figure 4.2(b), with various $(\gamma_{11},\gamma_{22})$, the ratio r_1/r_2 decreases as γ_{11}/γ_{22} becomes larger. More precisely, the two ratios satisfy the following law:

$$\frac{r_1}{r_2}=\left(\frac{\gamma_{11}}{\gamma_{22}}\right)^{-\frac{1}{3}}. \tag{4.1}$$

This relationship can also be verified theoretically. Let K_1 be the number of red bubbles and K_2 be the number of yellow bubbles in a single bubble assembly. The full

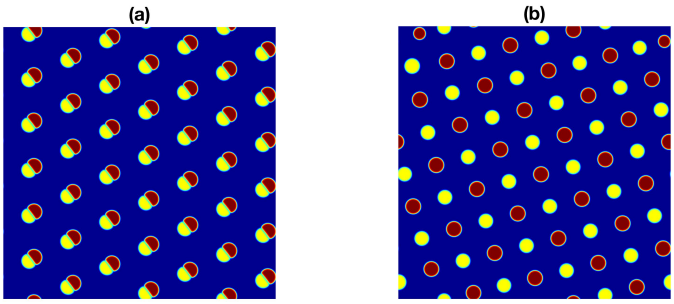

FIG. 4.1. *Two characteristic patterns in ternary systems. (a) A ternary system with* $\gamma_{12}=0$ *maintains a hexagonal double bubble assembly. (b) A system with* $\gamma_{12}=11{,}000$ *yields a single bubble assembly in a square lattice. The snapshots are taken at time* $T=400$. $\gamma_{11}=\gamma_{22}=20{,}000$, $\omega_1=0.10$, *and* $\omega_2=0.09$ *in these simulations.*

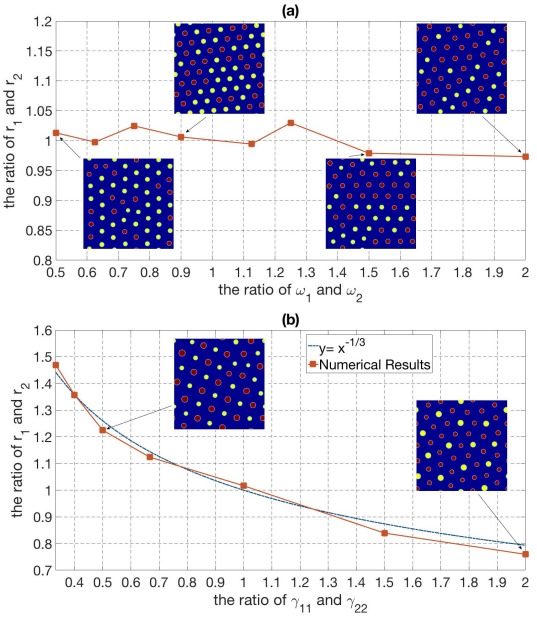

FIG. 4.2. *(a) Independence of the average red and yellow bubble sizes on the ratio of area fractions* ω_1/ω_2. *For* $(\omega_1,\omega_2)=(0.05,0.10)$, $(0.09,0.144)$, $(0.09,0.12)$, $(0.09,0.10)$, $(0.09,0.08)$, $(0.09,0.072)$, $(0.09,0.06)$, $(0.10,0.05)$, *the ratio* r_1/r_2 *remains at* $1/1$ *up to a* 3% *error. Here* $\gamma_{11}=\gamma_{12}=\gamma_{22}=20{,}000$. *(b) Dependence of the average red and yellow bubble sizes on the long-range interaction coefficients* γ_{11} *and* γ_{22}. *For* $(\gamma_{11},\gamma_{22})=(20{,}000,\ 60{,}000)$, $(20{,}000,\ 50{,}000)$, $(10{,}000,\ 20{,}000)$, $(20{,}000,\ 30{,}000)$, $(20{,}000,\ 20{,}000)$, $(30{,}000,\ 20{,}000)$, $(20{,}000,\ 10{,}000)$, *numerical simulations agree with the law of* $r_1/r_2=(\gamma_{11}/\gamma_{22})^{-1/3}$. *Here* $\gamma_{12}=20{,}000,\ 20{,}000,\ 10{,}000,\ 20{,}000,\ 10{,}000,\ 20{,}000,\ 10{,}000$ *respectively.* $(\omega_1,\omega_2)=(0.10,0.05)$, $(0,10,0.05)$, $(0.09,0.06)$, $(0.10,0.05)$, $(0.07,0.07)$, $(0.09,0.06)$, $(0.09,0.06)$ *respectively.*

form of the free energy of a single bubble assembly in the strong segregation limit is (2.14). In an equilibrium state, all red bubbles develop into approximately the same size; so do yellow bubbles. Let r_1 and r_2 be the average radii of red and yellow bubbles, respectively. Up to the leading order, the free energy is

$$\sum_{i=1}^{2} K_i \left(2\pi r_i + \frac{\gamma_{ii}\pi}{4} (r_i)^4 \log \frac{1}{r_i} \right). \tag{4.2}$$

Let $\eta^2 m = \omega_1 |D|$, $\eta^2(1-m) = \omega_2 |D|$, and $\Gamma_{ij} = \eta^3 \log \frac{1}{\eta} \gamma_{ij}$. Then (4.2) becomes

$$\eta\left(2\sqrt{m\pi}K_1^{\frac{1}{2}} + \frac{\Gamma_{11}m^2}{4\pi}K_1^{-1} + 2\sqrt{(1-m)\pi}K_2^{\frac{1}{2}} + \frac{\Gamma_{22}(1-m)^2}{4\pi}K_2^{-1}\right).$$

With respect to K_1 and K_2 the above is minimized at

$$K_1 = \left(\frac{\Gamma_{11}}{4}\right)^{\frac{2}{3}} \frac{m}{\pi},\ K_2 = \left(\frac{\Gamma_{22}}{4}\right)^{\frac{2}{3}} \frac{1-m}{\pi}.$$

Consequently the average radii of red and yellow bubbles, are

$$r_i = 4^{\frac{1}{3}} \left(\log \frac{1}{\eta}\right)^{-\frac{1}{3}} \gamma_{ii}^{-\frac{1}{3}},\ i = 1,2, \tag{4.3}$$

from which (4.1) follows.

4.3. Double bubble assemblies. In some parameter ranges, ternary systems may display double bubble assemblies (see Figure 4.1 (a)). Let $\omega_1 = \omega_2 = 0.09$, $\gamma_{12} = 0$, and increase $\gamma_{11} = \gamma_{22}$ from 200 to 40,000. The number of double bubbles K_b in an assembly increases correspondingly as seen in the insets of Figure 4.3(a). The increment of K_b obeys the law $K_b \sim \gamma_{11}^{2/3}$. This confirms that the long-range interaction favors small domains.

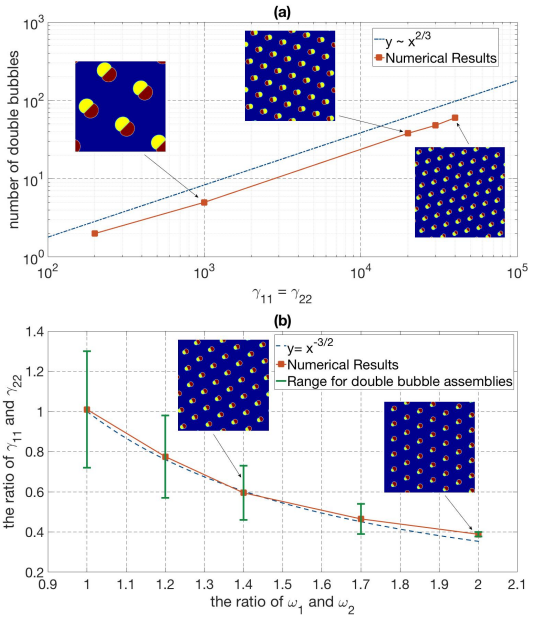

FIG. 4.3. *(a) Log-log plot of the dependence of the number of double bubbles on γ_{11} in symmetric double bubble assemblies. Here $\gamma_{11} = \gamma_{22}$, $\gamma_{12} = 0$, and $\omega_1 = \omega_2 = 0.09$. As γ_{11} increases, the number of double bubbles in the assemblies grows accordingly. For $\gamma_{11} = 200$, 1,000, 20,000, 30,000, 40,000, the corresponding number of double bubbles are 2, 5, 38, 48 and 60, respectively. (b) The range of γ_{11}/γ_{22} under which random initials evolve to double bubble assemblies for given ω_1 and ω_2. For $(\omega_1, \omega_2) =$ (0.09,0.09), (0.09,0.09/1.2), (0.09,0.09/1.4), (0.10,0.10/1.7), (0.10,0.05), the ranges of γ_{11}/γ_{22} are (0.72,1.3), (0.57,0.98), (0.46,0.73), (0.39,0.54), and (0.3774,0.40) respectively. Here $\gamma_{12} = 0$.*

This two-thirds law can be verified theoretically for both symmetric ($\omega_1 = \omega_2$) and asymmetric ($\omega_1 \neq \omega_2$) double bubble assemblies. To this end, consider the strong segregation limit of the free energy E [27]. The full form of the free energy of a double bubble assembly in the strong segregation limit is (2.15). In an equilibrium state, all double bubbles have approximately the same shape and size. Let l_i, $i = 0,1,2$, denote the radii of the three arcs of a double bubble whose two areas are $\frac{m}{K_b}$ and $\frac{1-m}{K_b}$. Let a_i, $i = 0,1,2$, denote the angles associated with these arcs. Up to the leading order, the free energy is

$$K_b \left(\sum_{i=0}^{2} a_i l_i \eta + \sum_{i,j=1}^{2} \frac{\gamma_{ij}}{4\pi} \left(\eta^4 \log \frac{1}{\eta} \right) \frac{m_i m_j}{K_b^2} \right), \tag{4.4}$$

where $\eta^2 m = \omega_1 |D|$, $\eta^2 (1-m) = \omega_2 |D|$, $m_1 = m$, and $m_2 = 1-m$. If L_i, $i = 0,1,2$, are the radii of the three arcs of a double bubble whose two areas are m and $1-m$, then $l_i = L_i / \sqrt{K_b}$. Let $\Gamma_{ij} = \eta^3 \log \frac{1}{\eta} \gamma_{ij}$ and rewrite (4.4) as

$$\eta \left[\left(\sum_{i=0}^{2} a_i L_i \right) K_b^{\frac{1}{2}} + \left(\sum_{i,j=1}^{2} \frac{\Gamma_{ij} m_i m_j}{4\pi} \right) K_b^{-1} \right].$$

With respect to K_b, this is minimized at

$$K_b = \left(\frac{\sum_{i,j=1}^{2} \Gamma_{ij} m_i m_j}{2\pi \sum_{i=0}^{2} a_i L_i} \right)^{\frac{2}{3}}. \tag{4.5}$$

Figure 4.3(b) shows the relationship between γ_{11}/γ_{22} and ω_1/ω_2 when double bubble assemblies occur. The vertical green line for each value of ω_1/ω_2 indicates the range of γ_{11}/γ_{22} for which double bubble assemblies exist. Beyond this range, ternary systems display other patterns such as coexisting single and double bubbles. The range becomes wider when ω_1/ω_2 approaches 1. Taking γ_{11}/γ_{22} to be the middle value in each range, and plotting it with respect to the ratio ω_1/ω_2, one finds that it agrees with the graph of $y = x^{-3/2}$.

4.4. The effect of γ_{12}. As γ_{12} increases from 0, red and yellow constituents tend to break. In Figure 4.4(a), $\gamma_{12} = 0$ and all components are double ones. In Figure 4.4(b), $\gamma_{12} = 8{,}000$, many double bubbles break into single red and yellow bubbles to yield a coexisting pattern. In Figure 4.4(c), $\gamma_{12} = 10{,}000$, all double bubbles disappear, the assembly becomes a pure single bubble one. In this case the red and yellow bubbles are well mixed in an organized way. In Figure 4.4(d), $\gamma_{12} = 20{,}000$, the system still displays a single bubble assembly, but the red and yellow bubbles are mixed randomly; many single bubbles of the same color gather together. When $\gamma_{12} = 22{,}000$ is even larger in Figure 4.4(e), red bubbles are completely separated from yellow bubbles in the assembly. Note that as γ_{12} increases, the matrix γ changes from being positive definite, to semi-positive definite, and to indefinite. In Figure 4.4(f), a negative γ_{12} is used. Red and yellow constituents tend to be more "adhesive". Nonstandard double bubbles appear in the assembly. In Figure 4.5, the numbers of single and double bubbles when γ_{12} changes from 0 to 10,000 are recorded. The existence of double bubble assemblies and single bubble assemblies have been theoretically established recently [32,34]. There have been no theoretical studies on assemblies of coexisting single and double bubbles or on assemblies of nonstandard double bubbles.

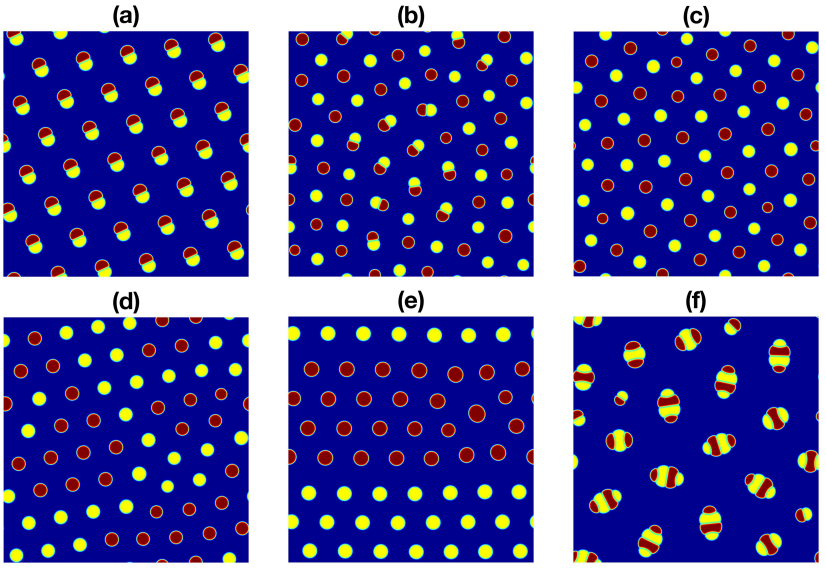

FIG. 4.4. *The effect of* γ_{12}. *As* γ_{12} *increases, double bubble assemblies change to coexisting single and double bubbles, and then to single bubble assemblies. When* γ_{12} *is negative, nonstandard double bubbles appear. (a)* $\gamma_{12}=0$, *(b)* $\gamma_{12}=8{,}000$, *(c)* $\gamma_{12}=10{,}000$, *(d)* $\gamma_{12}=20{,}000$, *(e)* $\gamma_{12}=22{,}000$, *and (f)* $\gamma_{12}=-13{,}000$. *The other parameters are* $\gamma_{11}=\gamma_{22}=20{,}000$, $\omega_1=\omega_2=0.09$.

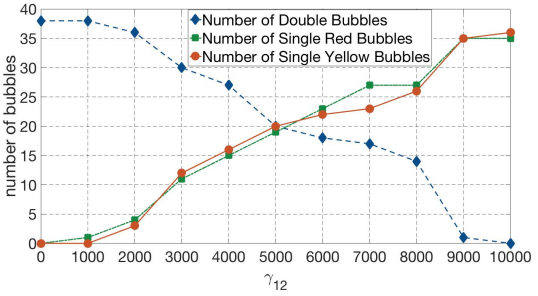

FIG. 4.5. *The numbers of bubbles as* γ_{12} *increases from* 0 *to* 10,000. *The other parameters are* $\gamma_{11}=\gamma_{22}=20{,}000$, $\omega_1=\omega_2=0.09$.

5. Conclusion

We explore the dynamics of bubble assemblies via the gradient flow of a nonlocal energy functional modeling the self-assembly of triblock copolymers in ternary systems with small volume fractions of two constituents. Here for numerical simulations we focus attention on the diffuse interface approach. Meanwhile, we also use the sharp interface limit, the nonlocal two-component isoperimetric functional, to provide theoretical verification of the quantitative studies. In the diffuse interface model, we introduce the term $f(\phi)=3\phi^2-2\phi^3$ to localize the 'boundary force' near the A-C, B-C and A-B interfaces. In developing the numerical method for the gradient-flow dynamics, we first adopt a linear splitting scheme to reformulate the coupled nonlocal Allen-Cahn equations, and then use the semi-implicit scheme to discretize the time variable and the spectral method to discretize the space variables. In the sharp interface model, we derive the leading order of the free energy via asymptotic analysis. Numerical simulations answered one

open question from the theoretical study of triblock copolymers: the polarity direction of double bubbles in double bubble assemblies should be parallel. Moreover, it is shown both numerically and theoretically that the average size of red/yellow bubbles in a single bubble assembly does not depend on ω_1/ω_2, the ratio of the area fractions of the minority constituents, but rather on γ_{11} and γ_{22}, as well as $\omega_1+\omega_2$ and the number of double bubbles in a double bubble assembly satisfies a two-thirds power law. A relationship between γ_{11}/γ_{22} and ω_1/ω_2 is also identified for double bubble assemblies.

This work can be extended in a number of directions. Morphological patterns in three dimensions can be studied by the same model. It can also be generalized for quaternary systems, such as tetrablock copolymers. Other gradient flows of E, such as a H^{-1} flow which leads to nonlocal Cahn-Hilliard system of equations, are also worth studying.

Acknowledgements. X.R. is supported by National Science Foundation, DMS-1714371. Y.Z. is supported by a grant from the Simons Foundation through Grant No. 357963.

REFERENCES

[1] F.S. Bates and G.H. Fredrickson, *Block copolymers - designer soft materials*, Phys. Today, 52(2):32, 1999. 1

[2] I.W. Hamley, *Developments in Block Copolymer Science and Technology*, Wiley, New York, 2004. 1

[3] I. Botiz and S.B. Darling, *Optoelectronics using block copolymers*, Mater. Today, 13(5):42–51, 2010. 1

[4] M. Takenaka, T. Wakada, S. Akasaka, S. Nishitsuji, K. Saijo, H. Shimizu, M.I. Kim and H. Hasegawa, *Orthorhombic Fddd network in diblock copolymer melts*, Macromolecules, 40(13):4399–4402, 2007. 1

[5] E. Helfand and Z.R. Wasserman, *Block copolymer theory. 4. Narrow interphase approximation*, Macromolecules, 9(6):879–888, 1976. 1

[6] M.W. Matsen and M. Schick, *Stable and unstable phases of a diblock copolymer melt*, Phys. Rev. Lett., 72:2660, 1994. 1

[7] F. Drolet and G.H. Fredrickson, *Combinatorial screening of complex block copolymer assembly with self-consistent field theory*, Phys. Rev. Lett., 83:4317, 1999. 1

[8] C.A. Tyler, J. Qin, F.S. Bates, and D.C. Morse, *SCFT study of nonfrustrated ABC triblock copolymer melts*, Macromolecules, 40(13):4654–4668, 2007. 1

[9] Z. Guo, G. Zhang, F. Qiu, H. Zhang, Y. Yang and A.C. Shi, *Discovering ordered phases of block copolymers: new results from a generic Fourier-space approach*, Phys. Rev. Lett., 101:028301, 2008. 1

[10] X. Cheng, L. Lin, W. E., P. Zhang, A.C. Shi, *Nucleation of ordered phases in block copolymers*, Phys. Rev. Lett., 104:148301, 2010. 1

[11] Y. Jiang and J.Z.Y. Chen, *Influence of chain rigidity on the phase behavior of wormlike diblock copolymers*, Phys. Rev. Lett., 110:138305, 2013. 1

[12] Y. Oono and Y. Shiwa, *Computationally efficient modeling of block copolymer and Benard pattern formations*, Mod. Phys. Lett. B, 01:49, 1987. 1

[13] M. Bahiana and Y.Oono, *Cell dynamical system approach to block copolymers*, Phys. Rev. A, 41:6763, 1990. 1, 1

[14] S.R. Ren and I.W. Hamley, *Cell dynamics simulations of microphase separation in block copolymers*, Macromolecules, 34(1):116, 2001. 1

[15] X.-F. Wu and Y.A. Dzenis, *Phase-field modeling of the formation of lamellar nanostructures in diblock copolymer thin films under inplanar electric fields*, Phys. Rev. E, 77:031807, 2008. 1

[16] T. Ohta and K. Kawasaki, *Equilibrium morphology of block copolymer melts*, Macromolecules, 19(10):2621, 1986. 1, 1, 4.1

[17] H. Nakazawa and T. Ohta, *Microphase separation of ABC-type triblock copolymers*, Macromolecules, 26(20):5503–5511, 1993. 1, 4.1

[18] X. Ren and J. Wei, *Triblock copolymer theory: free energy, disordered phase and weak segregation*, Phys. D, 178(1-2):103–117, 2003. 1

[19] R. Choksi and X. Ren, *Diblock copolymer/homopolymer blends: derivation of a density functional theory*, Phys. D, 203(1-2):100–119, 2005. 1
[20] Y. Zhao, Y. Ma, H. Sun, B. Li, and Q. Du, *A new phase-field approach to variational implicit solvation of charged molecules with the Coulomb-field approximation*, Commun. Math. Sci., 16:1203–1123, 2018. 1, 3.2
[21] X. Xu and Y. Zhao, *Energy stable semi-implicit schemes for Allen-Cahn-Ohta-Kawasaki model in binary system*, J. Sci. Comput., 80(3):1656–1680, 2019. 1
[22] X. Wang, L. Ju, and Q. Du, *Efficient and stable exponential time differencing Runge-Kutta methods for phase field elastic bending energy models*, J. Comput. Phys., 316:21–38, 2016. 1, 3.2
[23] E. De Giorgi, *Sulla convergenza di alcune successioni d'integrali del tipo dell'area*, Rend. Mat., 6(8):277–294, 1975. 1
[24] L. Modica and S. Mortola, *Un esempio di* Γ*-convergenza.*, Boll. Un. Mat. Ital. B(5), 14(1):285–299, 1977. 1
[25] L. Modica, *The gradient theory of phase transitions and the minimal interface criterion*, Arch. Ration Mech. Anal., 98(2):123–142, 1987. 1
[26] R.V. Kohn and P. Sternberg, *Local minimisers and singular perturbations*, Proc. Roy. Soc. Edinburgh Sect. A, 111(1-2):69–84, 1989. 1
[27] S. Baldo, *Minimal interface criterion for phase transitions in mixtures of Cahn-Hilliard fluids*, Ann. Inst. Henri. Poincaré, 7-2:67–90, 1990. 1, 4.3
[28] X. Ren and J. Wei, *On the multiplicity of solutions of two nonlocal variational problems*, SIAM J. Math. Anal., 31(4):909–924, 2000. 1
[29] L.C. Evans and R.F. Gariepy, *Measure Theory and Fine Properties of Functions*, CRC Press, Boca Raton, FL, 1992. 2
[30] E. Giusti, *Minimal Surfaces and Functions of Bounded Variation*, Birkhäuser, 1984. 2
[31] W.P. Ziemer, *Weakly Differentiable Functions: Sobolev Spaces and Functions of Bounded Variation*, Springer, New York, 2002. 2
[32] X. Ren and J. Wei, *A double bubble assembly as a new phase of a ternary inhibitory system*, Arch. Ration. Mech. Anal., 215(3):967–1034, 2015. 2, 2.2, 4.1, 4.4
[33] X. Ren and C. Wang, *A stationary core-shell assembly in a ternary inhibitory system*, Discrete Contin. Dyn. Syst., 37(2):983–1012, 2017. 2
[34] X. Ren and C. Wang, *Stationary disk assemblies in a ternary system with long range interaction*, Commun. Contemp. Math., 21(6):1850046, 2019. 2, 2.1, 2, 4.4
[35] D. Gilbarg and S.N. Trudinger, *Elliptic Partial Differential Equations of Second Order*, Springer-Verlag, Berlin, Heidelberg, New York, Tokyo, Second Edition, 1983. 2
[36] Q. Du and W. Zhu, *Analysis and applications of the exponential time differencing schemes and their contour integration modifications*, BIT Numer. Math., 45(2):307–328, 2005. 3.2
[37] L. Ju, J. Zhang, L. Zhu, and Q. Du, *Fast explicit integration factor methods for semilinear parabolic equations*, J. Sci. Comput., 62(2):431–455, 2015. 3.2
[38] C. Xu and T. Tang, *Stability analysis of large time-stepping methods for epitaxial growth models*, SIAM J. Numer. Anal., 44(4):1759–1779, 2006. 3.2
[39] C.V. Loan, *Computational Frameworks for the Fast Fourier Transform*, SIAM, Philadelphia, 1992. 3.3
[40] T. Hashimoto, H. Tanaka, and H. Hasegawa, *Morphology control through phase transitions in two-component polymer systems*, in M. Nagasawa (ed.), Molecular Conformation and Dynamics of Macromolecules in Condensed Systems, Elsevier Science, 2, 1988. 4.1
[41] E. Helfand and Z.R. Wasserman, *Block copolymer theory. 6. Cylindrical domains*, Macromolecules, 13(4):994–998, 1980. 4.1
[42] L. Leibler, *Theory of microphase separation in block copolymers*, Macromolecules, 13(6):1602–1617, 1980. 4.1
[43] X. Chen and Y. Oshita, *An application of the modular function in nonlocal variational problems*, Arch. Ration. Mech. Anal., 186(1):109–132, 2007. 4.1
[44] X. Ren and J. Wei, *Many droplet pattern in the cylindrical phase of diblock copolymer morphology*, Rev. Math. Phys., 19(08):879, 2007. 4.1
[45] C. Tang, J. Bang, G.E. Stein, G.H. Fredrickson, C.J. Hawker, E.J. Kramer, M. Sprung and J. Wang, *Square packing and structural arrangement of ABC triblock copolymer spheres in thin films*, Marcromolecules, 41(12):4328–4339, 2008. 4.1
[46] W. Zheng and Z.-G. Wang, *Morphology of ABC triblock copolymers*, Macromolecules, 28(21):7215–7223, 1995. 4.1
[47] P. Tang, F. Qiu, H. Zhang, and Y. Yang, *Morphology and phase diagram of complex block copolymers: ABC linear triblock copolymers*, Phys. Rev. E, 69:031803, 2004. 4.1
[48] S. Luo, X. Ren, and J. Wei, *Non-hexagonal lattices from a two species interacting system*, arXiv:1902.09611. 4.1